MRI Signal Reconstruction via Fourier Frames on Interleaving Spirals
Mid-Year Report

Christiana Sabett
Applied Mathematics, Applied Statistics, & Scientific Computation

Advisors: John Benedetto, Alfredo Nava-Tudela
Mathematics, IPST

December 14, 2015

1 Abstract

This project aims to effectively reconstruct an MRI signal using Fourier frames. We begin by describing the theoretical framework of a Fourier frame on the Paley-Wiener space $PW_{\overline{B(0,R)}}$. We then invoke Beurling's theorem to prove that we can choose points along interleaving spirals in the spectral domain to construct a Fourier frame for $PW_{\overline{B(0,R)}}$. We use frame notation to extend these results to the signal space of a square image, forming a reconstruction algorithm that results in an overdetermined linear system. We implement two different algorithms to solve the least-squares approximation in order to recover the spatial components of the MRI signal.

2 Background

MRI signal reconstruction from spectral sampling is a common problem in the field of signal processing. Formally stated, image reconstruction is an inversion problem: given frequency information, we want to recover the spatial components of the image. MRI reconstruction in particular desires both speed and accuracy, but often the former is neglected. Previous results have shown that sampling on interleaving spirals in the spectral domain makes for much faster data acquisition than rectilinear spectral sampling [8, 5]. We desire a reconstruction scheme that makes use of this data acquisition method. The standard approach to MRI reconstruction relies on uniform sampling of the spectral domain [11]. We will show that by sampling nonuniformly along the interleaving spirals, we can construct a Fourier frame approximant that allows us to achieve perfect MRI reconstruction.

It is well-established that uniform sampling in the spectral domain of a band-limited signal can produce perfect reconstruction (Shannon's theorem), i.e. the reconstructed signal is a scaled, delayed version of the original signal. This result leads to the Nyquist sampling theorem, which states that to obtain perfect reconstruction, a band-limited signal must be sampled at a rate at least twice the maximum frequency [11]. Rectilinear sampling in the spectral domain consists of points (λ, μ) where $\lambda = mh_\lambda$ and $\mu = nh_\mu$ for $m, n \in \mathbb{Z}$ and for fixed distances between coordinates h_λ and h_μ that satisfy the Nyquist criterion. The typical MRI reconstruction algorithm samples rectilinearly and then applies the Fast Fourier Transform to recover the image [6, 11].

A standard MRI machine measures the exact spectral components of the signal. Coils generate a magnetic field that causes the body's protons to align with it along a magnetic vector. A radio wave frequency (RF) is then passed through the body to disrupt the magnetic field, forcing the protons out of equilibrium. Once the pulse passes, the protons realign with the magnetic field. The time it takes for the particles to return

to homeostasis and the amount of energy released indicate the type of tissue the pulses are moving through. Localizing the magnetic field allows for the recovery of images such as Figure 1 [4, 12].

Figure 1: "Carolyn's MRI", by ClintJCL (Flickr)

3 Theoretical Approach

The *Paley-Wiener space* PW_E is defined as

$$PW_E = \{\varphi \in L^2(\widehat{\mathbb{R}}^d) : \text{supp } \varphi^\vee \subseteq E\},$$

where $\widehat{\mathbb{R}}^d$ is the domain of the Fourier transforms of signals in d-dimensional Euclidean space, and $L^2(\widehat{\mathbb{R}}^d)$ is the space of finite energy signals on $\widehat{\mathbb{R}}^d$ with $E \subseteq \mathbb{R}^d$ compact. The Fourier transform of a signal $f(x)$ is defined as $\mathcal{F} : L^2(\mathbb{R}^d) \to L^2(\widehat{\mathbb{R}}^d)$ such that $\mathcal{F}(f)(\omega) = \int_{-\infty}^{\infty} f(x)e^{-2\pi ix\cdot\omega}dx$. $\varphi^\vee$ denotes the inverse Fourier transform of φ and supp $\varphi^\vee$ denotes the support of $\varphi^\vee$ [3].

In a separable Hilbert space H, a *frame* is defined as a sequence $\{x_n : n \in \mathbb{Z}^d\} \subseteq H$ for which there exist $A, B > 0$ such that

$$\forall y \in H, \quad A||y||^2 \leq \sum_n |\langle y, x_n\rangle|^2 \leq B||y||^2.$$

Let $\Lambda \subseteq \widehat{\mathbb{R}}^d$ be a sequence and let $E \subseteq \mathbb{R}^d$ be compact. Define the sequence $\{e_\lambda \mathbb{1}_E : \lambda \in \Lambda\} \subseteq L^2(\mathbb{R}^d)$, where $e_\lambda(x) = e^{-2\pi ix\cdot\lambda}$. In particular, note that $(e_\lambda \mathbb{1}_E)^\wedge \in PW_E$ and $L^2(E) = (PW_E)^\vee$. The sequence $\{e_\lambda \mathbb{1}_E\}$ is a frame for $L^2(E)$ (where we write $L^2(E) \subseteq L^2(\mathbb{R}^d)$ because $(PW_E)^\vee \subseteq L^2(\mathbb{R}^d)$), if and only if there exist $0 < A \leq B < \infty$ such that

$$\forall f \in L^2(E), \quad A||f||^2_{L^2(E)} \leq \sum_{\lambda\in\Lambda} |\langle f, e_\lambda \mathbb{1}_E\rangle_{L^2(E)}|^2 \leq B||f||^2_{L^2(E)}$$

where $\langle f, e_\lambda \mathbb{1}_E\rangle_{L^2(E)} = \int_E f(x)e^{-2\pi ix\cdot\lambda}dx = \widehat{f}(\lambda)$. We can further say that the sequence $(e_\lambda \mathbb{1}_E)^\wedge$ is a frame for PW_E if $\{e_\lambda \mathbb{1}_E\}$ is a frame for $L^2(E)$. We call such a sequence a *Fourier frame for* PW_E [1, 3].

A set Λ is *uniformly discrete* if there exists $r > 0$ such that

$$\forall \lambda, \gamma \in \Lambda, \quad |\lambda - \gamma| \geq r.$$

When E is the closed ball $\overline{B(0,R)} \subset \mathbb{R}^d$ centered at $\mathbf{0}$ with radius R, Beurling's theorem tells us the following [3]: Let $\Lambda \subseteq \widehat{\mathbb{R}}^d$ be uniformly discrete and let $\text{dist}(\xi, \Lambda) = \inf_{\lambda \in \Lambda} \sqrt{\sum_{i=1}^d |\xi_i - \lambda_i|^2}$ denote the Euclidean distance between the point ξ and the set Λ. Define

$$\rho = \rho(\Lambda) = \sup_{\xi \in \widehat{\mathbb{R}}^d} \text{dist}(\xi, \Lambda).$$

If $R\rho < \frac{1}{4}$, then Λ is a Fourier frame for $PW_{\overline{B(0,R)}} \subseteq L^2(\widehat{\mathbb{R}}^d)$.

Define $L : L^2(E) \to \ell^2(\Lambda)$ of a Bessel map such that $f \to \{\widehat{f}(\lambda) : \lambda \in \Lambda\}$. Let L^* be its adjoint, and define the frame operator

$$S = L^*L : L^2(E) \to L^2(E)$$

such that $f \to S(f) = \sum_{\lambda \in \Lambda} \widehat{f}(\lambda) e_\lambda \mathbb{1}_E$. If $\{e_\lambda \mathbb{1}_E\}$ is a frame for $L^2(E)$, then

$$f = SS^{-1}f = \sum_{\lambda \in \Lambda} (S^{-1}f)^\wedge(\lambda) e_\lambda \mathbb{1}_E. \tag{1}$$

From this we can conclude that every finite energy signal $f \in L^2(E)$ can be represented as

$$f(x) = \sum_{\lambda \in \Lambda} a_\lambda(f) e_\lambda \mathbb{1}_E \tag{2}$$

in $L^2(\mathbb{R}^d)$, where $a_\lambda(f) = (S^{-1}f)^\wedge(\lambda)$ and $\sum_{\lambda \in \Lambda} |a_\lambda(f)|^2$ is finite.

Given the representation in (2), we must now choose a sequence $\Lambda_R \in \widehat{\mathbb{R}}^d$ such that Λ_R is a Fourier frame for $PW_{\overline{B(0,R)}}$. Let $c, R > 0$, and let $\{A_k : k = 0, 1, ..., m-1\}$ denote a finite set of interleaving Archimedean spirals of the form

$$A_k = \{c\theta e^{2\pi i(\theta - (k/m))} : \theta \geq 0\}.$$

Let $B = \cup_{k=1}^{m-1} A_k$. We will construct a uniformly discrete set $\Lambda_R \subseteq B$ that will form a Fourier frame for $PW_{\overline{B(0,R)}}$.

First, choose m such that $\frac{cR}{m} < 1/2$. For any given $\xi_0 \in \widehat{\mathbb{R}}^2$, we will write it as $\xi_0 = r_0 e^{2\pi i \theta_0}$ where $r_0 \geq 0$ and $\theta_0 \in [0, 1)$. Then either $0 \leq r_0 < c\theta_0 < c$ or there exists $n_0 \in \mathbb{N} \cup \{0\}$ for which

$$c(n_0 + \theta_0) \leq r_0 < c(n_0 + 1 + \theta_0).$$

In the second case, we can find $k \in \{0, \cdots, m-1\}$ such that

$$c(n_0 + \theta_0 + \frac{k}{m}) \leq r_0 < c(n_0 + \theta_0 + \frac{k+1}{m}),$$

which implies

$$\text{dist}(\xi_0, B) \leq \frac{c}{2m}.$$

Next, choose $\delta > 0$ such that $R\rho < 1/4$, where $\rho = (c/2m) + \delta$. For each k, we choose a uniformly discrete set of points Λ_k along the spiral A_k, where the curve distance between consecutive points is less than 2δ, beginning within 2δ of the origin. This rule guarantees that the distance from any point on the spiral A_k to Λ_k is less than δ. Finally, set $\Lambda_R = \cup_{k=0}^{m-1} \Lambda_k$. By the triangle inequality,

$$\begin{aligned} \forall \xi \in \widehat{\mathbb{R}}^2, \quad \text{dist}(\xi, \Lambda_R) &\leq \text{dist}(\xi, B) + \text{dist}(B, \Lambda_R) \\ &\leq \frac{c}{2m} + \delta = \rho. \end{aligned}$$

Recall that by our choices of δ and m, we have that $R\rho < 1/4$, thus Beurling's theorem tells us Λ_R is a Fourier frame for $PW_{\overline{B(0,R)}}$.

4 Problem

We shall extend the results in Section 3 to the signal space of a generic square image $f : \mathbb{R}^2 \to \mathbb{R}$ in a space $E \subseteq \mathbb{R}^2$ [3]. Consider the image $f \in L^2(E)$, taken to be zero outside of E. Let $\chi_1 = \{\square_k^1, p_k \in \square_k^1 \ \forall k\}_{k=0}^{B-1}$ be a refined tagged partition of E. We approximate f using the piecewise constant function f_{χ_1} due to lack of access to real MRI data. This approximation incurs an error ϵ between the true, smooth image f and the image f_{χ_1}. However, for any choice of ϵ, we can refine χ_1 such that $||f - f_{\chi_1}|| < \epsilon$, thus f_{χ_1} is a reasonable approximation of f. For a high-resolution image, the pixels act as the partition χ_1. Under this partition, the image has the representation

$$f_{\chi_1} = \sum_{k=0}^{B-1} f(p_k) \mathbb{1}_{\square_k^1} \tag{3}$$

and the equivalent spectral representation

$$\widehat{f_{\chi_1}} = \sum_{k=0}^{B-1} f(p_k) \widehat{\mathbb{1}}_{\square_k^1}. \tag{4}$$

Let $\chi_2 = \{\square_j^2, q_j \in \square_j^2 \ \forall j\}_{j=0}^{N_1 N_2 - 1}$ be a coarse tagged partition of E such that f_{χ_2} is piecewise constant. χ_2 is designed such that for each $q_j \in \chi_2$, there is a corresponding $p_k \in \chi_1$. Ideally, we would recover f_{χ_2} from the spectral information $\widehat{f}$ from the MRI machine. Computationally, we reconstruct f_{χ_2} given $\widehat{f_{\chi_1}}$, the approximation of $\widehat{f}$.

We restrict our view of the spectral domain to the square $\Omega \subseteq \widehat{\mathbb{R}}^2$, where the frame contribution outside the square is negligible. From our theoretical results, we can choose a set of points $\Lambda \subseteq \widehat{\mathbb{R}}^2$ along a set of interleaving spirals that gives rise to a Fourier frame for $L^2(E)$. Within the restricted domain Ω, we choose $M \geq N_1 N_2$ points $\alpha_i = (\lambda_i, \mu_i)$ for $i = 0, 1, ..., M-1$ on the interleaving spirals such that the α_i are nonuniform in the square. Let $\Lambda = \{\alpha_i\}$. We extend this tiling to the entire spectral domain by utilizing the periodic extension $\Lambda + K\mathbb{Z}^2$, giving rise to a frame $\{e_{\alpha_i}\}_{\alpha_i \in \Lambda}$ for PW_E, where $E = [-\frac{1}{2}, \frac{1}{2}]^2$. The MRI machine gathers true information about $\widehat{f}$. Thus, by specifying the points $\alpha_i \in \Lambda \cap \Omega$, we have access to $\{\widehat{f_{\chi_1}}(\alpha_i), i = 0, 1, ..., M-1\}$, the approximation of $\{\widehat{f}(\alpha_i)\}$, where we compute

$$\widehat{f_{\chi_1}}(\alpha_i) = \sum_{k=0}^{B-1} f(p_k) \widehat{\mathbb{1}}_{\square_k^1}(\alpha_i). \tag{5}$$

Let

$$g = \sum_{j=0}^{N_1 N_2 - 1} c_j \mathbb{1}_{\square_j^2} \tag{6}$$

be an image formed over the coarse partition χ_2. Given the spectral information $\widehat{f_{\chi_1}}(\alpha_i)$, we wish to find the image over the coarse partition that matches the frequency information of the high-resolution image at the points on the frame. To that end, we want to find c_j that solve

$$\min_c \sum_{i=0}^{M-1} |\widehat{f_{\chi_1}}(\alpha_i) - \widehat{g}(\alpha_i)|^2. \tag{7}$$

We then compare the actual recovered image g to the ideal recovered image f_{χ_2} formed by local averaging over the high-resolution image f_{χ_1}.

Let $H_j(\alpha_i) = \widehat{\mathbb{1}}_{\square_j^2}(\alpha_i)$. As the characteristic functions are separable by dimension, this is equivalent to $H_j(\alpha_i) = H_j(\lambda_i, \mu_i) = \widehat{\mathbb{1}}_{-\frac{2}{x_j}}(\lambda_i) \widehat{\mathbb{1}}_{-\frac{2}{y_j}}(\mu_i)$, where

$$H_j(\alpha_i) = H_j(\lambda_i, \mu_i) = \frac{1}{N_1} \frac{1}{N_2} \text{sinc}\left(\frac{1}{N_1} \lambda_i\right) \ \text{sinc}\left(\frac{1}{N_2} \mu_i\right) e^{-2\pi I (T_n \lambda_i + T_m \mu_i)} \tag{8}$$

We define $\text{sinc}(x)$ as the standard $\text{sinc}(x) = \frac{\sin \pi x}{\pi x}$, with $\text{sinc}(0)=1$, and (T_n, T_m) as the coordinates of the center of the current square, with $T_n = -\frac{1}{2} + \frac{2n+1}{2N_1}$ for $n \in \{0, ..., N_1 - 1\}$ and $T_m = -\frac{1}{2} + \frac{2m+1}{2N_2}$ for $m \in \{0, ..., N_2 - 1\}$. This gives

$$g(\alpha_i) = \sum_{j=0}^{N_1 N_2 - 1} c_j H_j(\alpha_i). \tag{9}$$

To minimize $|\widehat{f}_{\chi_1}(\alpha_i) - \widehat{g}(\alpha_i)|^2$, we set

$$\widehat{f}_{\chi_1}(\alpha_i) = \sum_{j=0}^{N_1 N_2 - 1} c_j H_j(\alpha_i). \tag{10}$$

Let

$$\widehat{\mathbb{F}} = [\widehat{f}_{\chi_1}(\alpha_0)\ \widehat{f}_{\chi_1}(\alpha_1)\ ...\ \widehat{f}_{\chi_1}(\alpha_{M-1})]^{\mathrm{T}}$$

and

$$\mathbb{F} = [c_0\ c_1\ ...\ c_{N_1 N_2 - 1}]^{\mathrm{T}}.$$

Define $\mathbb{H}$ such that $[\mathbb{H}]_{i,j} = H_j(\alpha_i)$, and (10) becomes

$$\widehat{\mathbb{F}} = \mathbb{H}\mathbb{F}. \tag{11}$$

The matrix equation (11) contains $M \geq N_1 N_2$ points in the spectral domain and $N_1 N_2$ points in the spatial domain. $\widehat{\mathbb{F}}$ is a length-M vector, $\mathbb{F}$ is a length-$N_1 N_2$ vector, and $\mathbb{H}$ is size $M \times N_1 N_2$. This yields an overdetermined system. $\mathbb{F}$ contains the spatial components of the image f that we wish to recover. In the following section, we will show that this matrix representation is equivalent to the frame reconstruction scheme.

5 Frame Reconstruction

The goal of this project is to use nonuniform sampling on interleaving spirals to define a Fourier frame in $\widehat{\mathbb{R}}^2$ from which we can reconstruct an image f. Recall that we do not have access to real MRI data, thus we use the spectral information over the fine partition χ_1 to recover the spatial components of our image f over a coarse partition χ_2. We create a synthetic data set using high-resolution images.

Given a high resolution image f_{χ_1}, generally of size 1024×1024, we form f_{χ_2}, an $N_1 \times N_2$ approximant, by averaging every $d \times d$ pixels of f_{χ_1}, where d is our reduction factor. The $N_1 \times N_2$ approximant f_{χ_2} is the optimal available image at that resolution. We take this as our ideal reconstruction, from which the error will be computed. From the high-resolution image f_{χ_1}, we sample $\widehat{f}_{\chi_1}(\alpha_i)$ as defined in (5) for $i = 0, 1, ..., M-1$ (with $M \geq N_1 N_2$) on a union of Archimedean spirals within the square Ω (Figure 2).

Beurling's theorem allows us to develop a reconstruction scheme using the set of points $\Lambda = \{\alpha_i\}$. The frame definition gives rise to a mapping $\mathbb{H}$ of $N_1 N_2$ points to M points, thus $\mathbb{H}$ is the matrix representation of the Bessel map $L : \ell^2(\{0, 1, ..., N_1 N_2 - 1\}) \to \ell^2(\{0, 1, ..., M-1\})$, $\mathbb{H}^*$ is its adjoint L^*, and $\mathbb{H}^*\mathbb{H}$ is equivalent to the frame operator $S = L^* L$. The frame reconstruction scheme is

$$g = (S^{-1} L^*) L g. \tag{12}$$

Setting $Lg = \widehat{f}_{\chi_1}$, our reconstructed image g takes the form

$$g = S^{-1} L^* \widehat{f}_{\chi_1}. \tag{13}$$

Applying the construction in Section 4 yields the overdetermined system in (11). We can see that in our frame terminology, the least-squares approximation

$$\mathbb{F} = (\mathbb{H}^*\mathbb{H})^{-1}\mathbb{H}^*\widehat{\mathbb{F}}, \tag{14}$$

where $\mathbb{H}^* := \overline{\mathbb{H}}^{\mathrm{T}}$, is equivalent to (12).

From g, we will compare our reconstruction with the optimal available image f_{χ_2} by analyzing $f_{\chi_2} - g$.

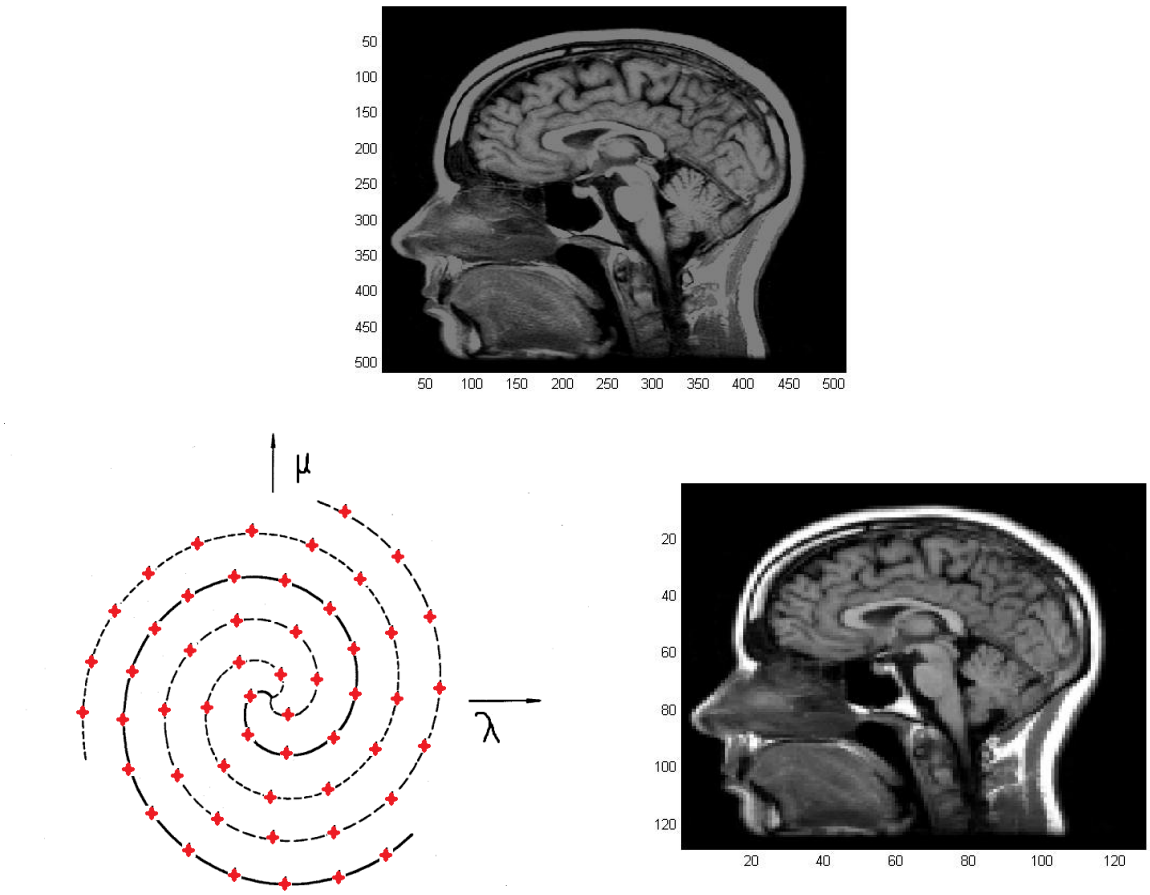

Figure 2: Problem overview. Top: High-resolution image f_{χ_1} from which synthetic data is formed. Bottom left: Sampling along interleaving spirals in the spectral domain of the high-resolution image. Bottom right: Downsampled version of the high-resolution image that serves as the ideal reconstruction.

6 Approach

A typical MRI image f is of size $N^2 = 256 \times 256$. This is the ultimate image size that we will attempt to reconstruct. Our primary concern is solving (14) to recover g by constructing $\widehat{\mathbb{F}}$ and $\mathbb{H}$ as described Section 4. Assuming $(\mathbb{H}^*\mathbb{H})^{-1}$ exists, g can be reconstructed. Note that $\mathbb{H}^*\mathbb{H}$ is fixed, which cuts down on storage costs considerably.

We will consider two reconstruction algorithms that solve the system

$$\mathbb{H}^*\mathbb{H}\mathbb{F} = \mathbb{H}^*\widehat{\mathbb{F}}. \tag{15}$$

The first is transpose reduction, which is the direct approach but with efficient storage. The second algorithm is the conjugate gradient method.

6.1 Transpose Reduction

This algorithm computes $\mathbb{H}^*\mathbb{H}$ directly as a sum of vector products instead of inefficiently storing $\mathbb{H}$ and then computing $\mathbb{H}^*\mathbb{H}$ [3, 7].

Define $V_i = (H_0(\alpha_i), ..., H_{N_1N_2-1}(\alpha_i))^*$ such that

$$\mathbb{H} = \begin{pmatrix} H_0(\alpha_0) & \cdots & H_{N_1N_2-1}(\alpha_0) \\ H_0(\alpha_1) & \cdots & H_{N_1N_2-1}(\alpha_1) \\ \vdots & \vdots & \vdots \\ H_0(\alpha_{M-1}) & \cdots & H_{N_1N_2-1}(\alpha_{M-1}) \end{pmatrix} = \begin{pmatrix} V_0^* \\ V_1^* \\ \vdots \\ V_{M-1}^* \end{pmatrix}.$$

Note that

$$\begin{aligned}
\mathbb{H}^*\mathbb{H} &= \begin{pmatrix} \sum_{i=0}^{M-1} \overline{H_0(\alpha_i)} H_0(\alpha_i) & \cdots & \sum_{i=0}^{M-1} \overline{H_0(\alpha_i)} H_{N_1N_2-1}(\alpha_i) \\ & \vdots & \\ \sum_{i=0}^{M-1} \overline{H_{N_1N_2-1}(\alpha_i)} H_0(\alpha_i) & \cdots & \sum_{i=0}^{M-1} \overline{H_{N_1N_2-1}(\alpha_i)} H_{N_1N_2-1}(\alpha_i) \end{pmatrix} \\
&= \sum_{i=0}^{M-1} \begin{pmatrix} \overline{H_0(\alpha_i)} H_0(\alpha_i) & \cdots & \overline{H_0(\alpha_i)} H_{N_1N_2-1}(\alpha_i) \\ & \vdots & \\ \overline{H_{N_1N_2-1}(\alpha_i)} H_0(\alpha_i) & \cdots & \overline{H_{N_1N_2-1}(\alpha_i)} H_{N_1N_2-1}(\alpha_i) \end{pmatrix} \\
&= \sum_{i=0}^{M-1} \begin{pmatrix} \overline{H_0(\alpha_i)} \\ \overline{H_1(\alpha_i)} \\ \vdots \\ \overline{H_{N_1N_2-1}(\alpha_i)} \end{pmatrix} (H_0(\alpha_i)\ H_1(\alpha_i)\ \cdots\ H_{N_1N_2-1}(\alpha_i)) \\
&= \sum_{i=0}^{M-1} V_i V_i^*.
\end{aligned}$$

Similarly,

$$\mathbb{H}^*\widehat{\mathbb{F}} = \begin{pmatrix} \sum_{i=0}^{M-1} \overline{H_0(\alpha_i)} \widehat{\mathbb{F}_i} \\ \vdots \\ \sum_{i=0}^{M-1} \overline{H_{N_1N_2-1}(\alpha_i)} \widehat{\mathbb{F}_i} \end{pmatrix} = \sum_{i=0}^{M-1} \widehat{\mathbb{F}_i} V_i.$$

To construct $A = \mathbb{H}^*\mathbb{H}$ and $b = \mathbb{H}^*\widehat{\mathbb{F}}$:

1. Let $V_0 = (H_0(\alpha_0), ..., H_{N_1N_2-1}(\alpha_0))^*$
2. Set $A = V_0V_0^*$ and $b = \widehat{f_0}V_0$
3. For $j = 1 : M-1$

   Set $V_j = (H_0(\alpha_j), ..., H_{N_1N_2-1}(\alpha_j))^*$
   $A \leftarrow A + V_jV_j^*$
   $b \leftarrow b + \widehat{f_j}V_j$

From here, (15) can be solved directly using a QR or Cholesky decomposition. This method uses a factor of N^2/M less memory than the direct approach with naive storage. In testing, as we increase the value of M, we expect this savings to become more apparent.

6.2 Conjugate Gradient Algorithm

Given the construction of $\mathbb{H}^*\mathbb{H}$,

$$[\mathbb{H}^*\mathbb{H}\mathbb{F}]_\ell = \sum_{j=0}^{N_1N_2-1} \mathbb{F}_j \sum_{i=0}^{M-1} \overline{H_\ell(\alpha_i) H_j(\alpha_i)},$$

where $[\mathbb{H}^*\mathbb{H}\mathbb{F}]_\ell$ denotes the ℓth element of $\mathbb{H}^*\mathbb{H}\mathbb{F}$. As in the Transpose Reduction algorithm, let $A = \mathbb{H}^*\mathbb{H}$ and $b = \mathbb{H}^*\widehat{\mathbb{F}}$. Then, for symmetric, positive definite A, we apply the conjugate gradient method [9] to solve the system $A\mathbb{F} = b$.

1. Choose f_0. Let $r_0 = b - Af_0$. Set $p_0 = r_0$.

2. for $n = 1$ until convergence

$$\gamma = (r_n^T r_n)/((Ap_n)^T p_n)$$
$$f_{n+1} = f_n + \gamma p_n$$
$$r_{n+1} = r_n - \gamma A p_n$$
$$\text{if norm}(r_{n+1}) < \text{tol, break}$$
$$\beta_n = (r_{n+1}^T r_{n+1})/(r_n^T r_n)$$
$$p_{n+1} = r_{n+1} + \beta_n p_n$$

This algorithm generally has linear convergence, but the speed of convergence depends on the condition number of A. We will also develop a modified implementation of the conjugate gradient algorithm that uses only matrix-vector operations instead of explicitly storing the matrix A.

7 Validation

7.1 Validation Methods

The following measures were used to evaluate the results.

7.1.1 PSNR

A standard measure of a reconstructed image is the peak signal-to-noise ratio (PSNR) [6]. It is defined in terms of the mean-squared error. Given our optimal available image f_{χ_2} of dimension $N_1 \times N_2$ and the reconstructed image g,

$$MSE = \frac{1}{N_1 N_2} \sum_{m=0}^{N_1-1} \sum_{n=0}^{N_2-1} (g(m,n) - f_{\chi_2}(m,n))^2$$

Then the PSNR, expressed in decibels (dB), is

$$PSNR = 10 \log \frac{max_{f_{\chi_2}}^2}{MSE} \tag{16}$$

where $max_{f_{\chi_2}}$ is the maximum possible pixel value for f_{χ_2}. As we are using purely grayscale images for this project, $max_{f_{\chi_2}} = 255$.

7.1.2 SSIM

The structural similarity (SSIM) index is a measure of similarity between two images [10]. Let x and y be signals where one is assumed to be of perfect quality. The luminance of each image is estimated by the mean intensities μ_x and μ_y. The standard deviations σ_x and σ_y are used to estimate the signal contrast. The constants C_1 and C_2 are used as stabilizers for when $\mu_x^2 + \mu_y^2$ and $\sigma_x^2 + \sigma_y^2$ are close to zero. The final form of the SSIM index is

$$\text{SSIM}(x,y) = \frac{(2\mu_x\mu_y + C_1)(2\sigma_{xy} + C_2)}{(\mu_x^2 + \mu_y^2 + C_1)(\sigma_x^2 + \sigma_y^2 + C_2)}.$$

7.2 Frame

The frame Λ was formed using the parameters $c = 1$, and $R = 0.5\frac{\sqrt{2}}{2}$ (half the diagonal of the square). It was constructed from one spiral and contained $2N_1N_2$ points in the complex plane.

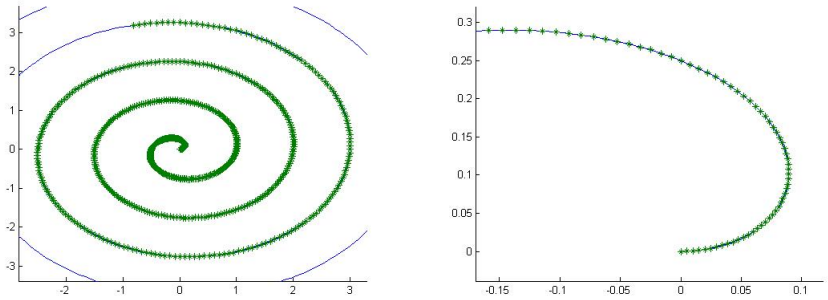

7.3 2x2 Recovery

A 2x2 low-resolution image was reproduced from high-resolution images of varying size. The frame Λ consisted of the points

Real(α_i)	Imag(α_i)
0	0.0050
0.0100	0.0149
0.0198	0.0247
0.0295	0.0342
0	0.0002
0.0006	0.0014
0.0025	0.0039
0.0056	0.0076

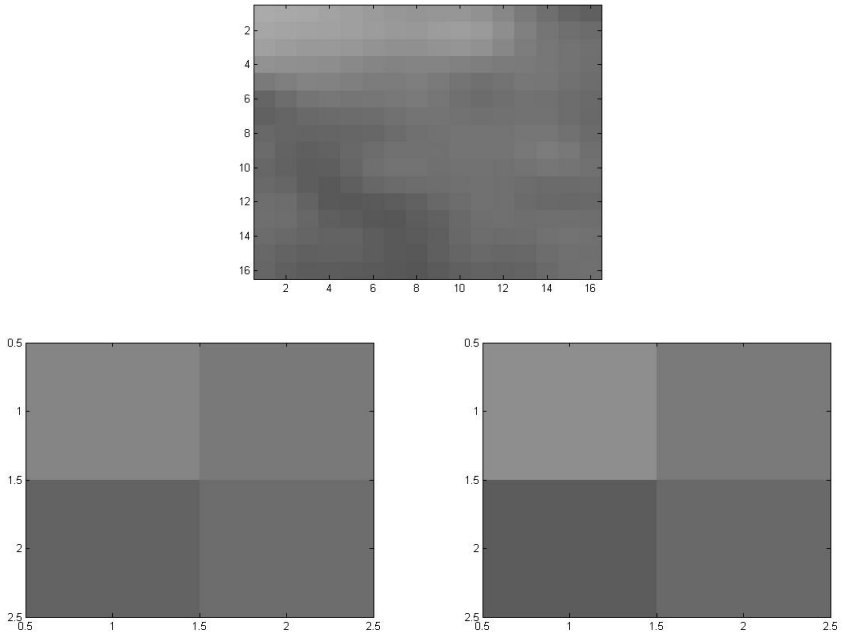

Figure 3: 2x2 reconstruction test. Top: 16x16 high-resolution image. Left: 2x2 ideal image. Right: 2x2 recovered image.

The results of reconstructing the image from a 16x16 high-resolution image are shown in Figure 3, with the accompanying details in the table below. This example showcases a reduction by a factor of eight in each dimension. We expect similar reductions for larger problems will be reasonable. The peak signal-to-noise ratio in this test was 32.4535 dB.

Ideal		Recovered	
132.6719	120.9063	142.0672	121.8891
98.6094	108.9688	91.8631	105.3507

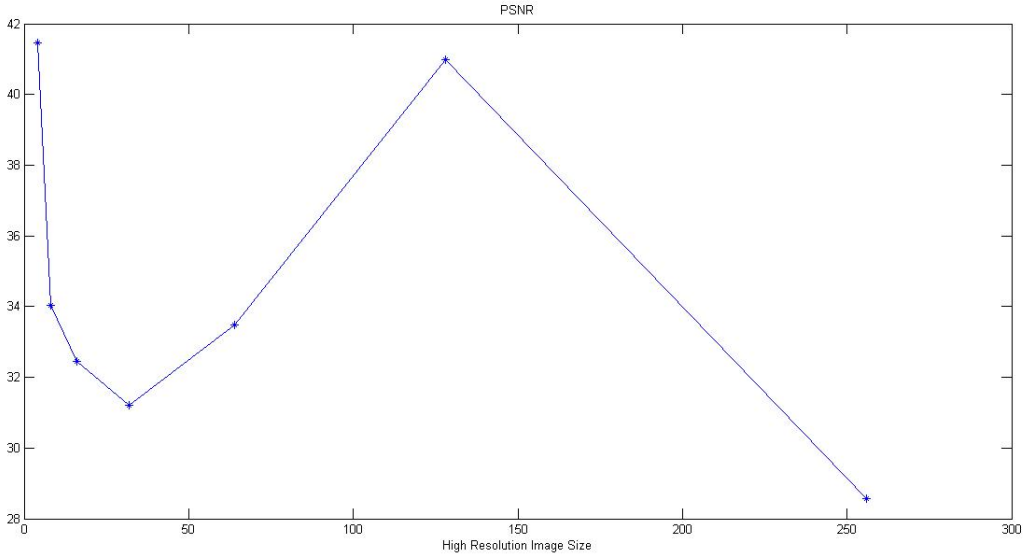

Figure 4: PSNR for 2x2 reconstruction test.

In total, seven tests were conducted, where a 2x2 matrix was reconstructed from high-resolution images of sizes $2^k \times 2^k$ for $k \in \{2, ...8\}$. The matrix $\mathbb{H}$ in each case is of dimension 8x4, corresponding to eight points in the frame and four pixels in the recovered image. The resulting PSNRs are shown in Figure 4. Note the PSNR began to increase starting with a high-resolution image of size 32x32. While this trend did not continue, it suggests that there may exist thresholds in which recovery would be maximized according to our ideal image. It is also important to note that for each trial, the minimum PSNR was still greater than 28 dB, at least double the PSNR we would see with recovery from a singular matrix.

More details are shown in the table below. Total error was calculated as the sum of the nominal differences between corresponding pixels of the ideal and recovered image. The average error per pixel stays within 4% of the ideal value.

HR Square Image Size	Total Error	Average Error Per Pixel	PSNR
4x4	7.9994	1.9999	41.4696
8x8	18.7343	4.6836	34.0317
16x16	20.7425	5.1856	32.4535
32x32	26.0165	6.5041	31.1978
64x64	19.4448	4.8612	33.4908
128x128	7.7677	1.9419	40.9905
256x256	36.6284	9.1571	28.5647

8 Future Work

Testing will continue in the form of larger problems. We will reconstruct larger low-resolution images from various size high-resolution images over the full data set. Still to be explored is the error convergence for different problem sizes, as well as how the condition number of $\mathbb{H}^*\mathbb{H}$ affects the reconstruction. Given that a frame consisting of $2N_1N_2$ points has been sufficient to reconstruct our 2x2 images, we expect this size frame is reasonable. It is also possible that we could reduce the size of the frame to N_1N_2 points, if this proves sufficient, in order to reduce computational time for larger problems.

9 Milestones

- Construct a Fourier frame via sampling on interleaving spirals.
- Implement the Transpose Reduction algorithm.
- Implement the conjugate gradient algorithm.

10 Timeline

- October 2015: Code the sampling routine to form the Fourier frame. [Complete]
- November 2015: Validation on small problems. [Complete]
- December 2015: Code the transpose reduction algorithm [Complete] and begin testing [Ongoing].
- January - February 2016: Code the conjugate gradient algorithm. Design and implement modified conjugate gradient algorithm.
- February - March 2016: Error analysis/testing. Explore how much frequency information we need to adequately recover f_{χ_2}. Explore condition number of $\mathbb{H}^*\mathbb{H}$ and how it affects the reconstruction.
- April 2016: Finalize results.

11 Deliverables

- Synthetic data set
- Fourier frame sampling routine
- Downsampling routine
- Routine to generate spectral data
- Transpose reduction routine
- Conjugate gradient routine
- Final report and error analysis

References

[1] Au-Yeung, Enrico, and John J. Benedetto. "Generalized Fourier Frames in Terms of Balayage." Journal of Fourier Analysis and Applications 21.3 (2014): 472-508.

[2] Benedetto, John J., and Hui C. Wu. "Nonuniform Sampling and Spiral MRI Reconstruction." Wavelet Applications in Signal and Image Processing VIII (2000).

[3] Benedetto, John J., Alfredo Nava-Tudela, Alex Powell, and Yang Wang. MRI Signal Reconstruction by Fourier Frames on Interleaving Spirals. Technical report. 2008.

[4] Berger, Abi. "Magnetic Resonance Imaging." BMJ : British Medical Journal. BMJ, 5 Jan. 2002. Web. 13 Oct. 2015.

[5] Bourgeois, Marc, Frank T. A. W. Wajer, Dirk Van Ormondt, and Danielle Graveron-Demilly. "Reconstruction of MRI Images from Non-Uniform Sampling and Its Application to Intrascan Motion Correction in Functional MRI." Modern Sampling Theory (2001): 343-63.

[6] I. Daubechies. *Ten Lectures on Wavelets.* Society for Industrial and Applied Mathematics, Philadelphia, PA, 1992.

[7] Goldstein, Thomas, Gavin Taylor, Kawika Barabin, and Kent Sayre. "Unwrapping ADMM: Efficient Distributed Computing via Transpose Reduction." Sub. 8 April 2015.

[8] Mansfield, P. "Multi-planar Image Formation Using NMR Spin Echoes." J. Phys. C: Solid State Phys. Journal of Physics C: Solid State Physics 10.3 (1977).

[9] O'Leary, Dianne P. Scientific Computing with Case Studies. Philadelphia: Society for Industrial and Applied Mathematics, 2009.

[10] Wang, Z., A.C. Bovik, H.R. Sheikh, and E.P. Simoncelli. "Image Quality Assessment: From Error Visibility to Structural Similarity." IEEE Transactions on Image Processing IEEE Trans. on Image Process. 13.4 (2004): 600-12.

[11] Yan, Hong. Signal Processing for Magnetic Resonance Imaging and Spectroscopy. New York: Marcel Dekker, 2002.

[12] "Magnetic Resonance Imaging (MRI)." Magnetic Resonance Imaging (MRI). NIH. Web. 13 Oct. 2015.